JOURNAL OF MATERIALS SCIENCE 31 (1996) 5101–5108

Metal distribution in alumina/aluminium composites synthesized by directed metal oxidation

H. VENUGOPALAN, T. DEBROY
Department of Materials Science and Engineering, Pennsylvania State University, University Park, PA 16802, USA

The directed oxidation of molten aluminium alloys by vapour phase oxidants can be used to produce Al_2O_3/Al ceramic matrix composites. The toughness of these composites is determined by the amount and the nature of metal distribution in the composite. This paper addresses the problem of understanding the metal distribution in Al_2O_3/Al composites and its dependence on growth temperature. Electrical conductivities and microstructures of Al_2O_3/Al composites synthesized by directed oxidation of Al-5056 alloy are investigated. The high conductivity of the Al_2O_3/Al composite compared to sintered Al_2O_3–4 wt% MgO is shown as a proof of the presence of some continuous metal channels in the composite. The activation energy for the diffusion of the dominant charge carrier in the oxide matrix is found to be 1.36 eV from the analysis of the conductivity data. Both the amount of metal in the composite and the extent of interconnection of the metal channels decrease with increasing growth temperature. The observed changes in microstructure with temperature can be explained by considering temperature variations of grain boundary energies in alumina and the alumina/aluminium interfacial energy. The metal content of the Al_2O_3/Al composites, prepared by directed oxidation of Al-5056 alloys, can be tailored by the choice of the growth temperature.

1. Introduction

In most structural applications, the primary disadvantage of ceramics is their lack of toughness. As a result, they are sensitive to sudden failure in response of accidental overloading, contact damage, or rapid temperature cycling. This deficiency has led to attempts to produce ceramic matrix composites which provide adequate toughness and other desirable properties. The directed oxidation of molten aluminium alloys by vapour phase oxidants can be used to produce tough ceramic matrix composites [1]. Fig. 1 illustrates schematically the formation of composite materials in this process. Under appropriate conditions of alloy composition, temperature and oxygen pressure, the molten alloy reacts rapidly with the oxidant to form α-alumina and the reaction product grows outwards from the original metal surface. The reaction is fed by the transport of liquid metal through the reaction product. The resulting material is a Al_2O_3/Al composite. Reinforced composites with desired structural properties can be obtained by growing the "composite" matrix into preforms consisting of reinforcing particulates, whiskers or fibres of Al_2O_3, SiC etc. [2–4]. Composites made by directed oxidation can be tailored to have good toughness, thermal shock resistance, wear resistance, high stiffness and high temperature stability. These composites are being evaluated for use in turbine engine components, armour applications, heat exchangers, and furnace components [5].

The directed oxidation of aluminium alloys depends crucially on certain alloying elements like magnesium and zinc [1, 6]. These elements form oxides (MgO and ZnO) at the surface, which prevent the passivation of the melt and facilitate the continuous supply of oxygen to the reaction interface. Three stages can be distinguished in the weight gain versus time curve, observed during the oxidation of Al–Mg alloys [7]. In the initial stage, rapid weight gain occurs owing to the formation of MgO [8]. MgO forms by oxidation of Mg vapour and subsequently falls back on to the melt surface [8]. Formation of a dense, thin layer of $MgAl_2O_4$ beneath the MgO halts the initial stage of oxidation and corresponds to the start of incubation [7]. During the second stage of incubation, metal channels are observed to form in the spinel and the arrival of these metal channels at the top of the spinel is believed to correspond to the end of incubation and the start of the growth stage [9]. During the final stage (growth), molten Al is believed to be transported by wicking (capillary action) from the bulk alloy to the top surface where oxidation of Al to Al_2O_3 occurs [10].

Several models have been proposed to explain the kinetics of oxidation of Al to Al_2O_3 in the growth stage. It has been suggested that during the growth

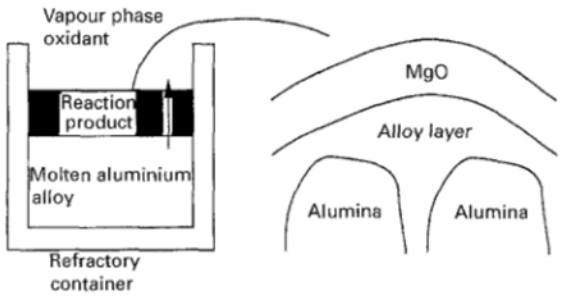

Figure 1 Schematic description of formation of ceramic matrix composites by the directed oxidation process.

stage of directed oxidation of Al–Mg alloys, a continuous MgO film exists at the top of the alumina matrix with a thin aluminium alloy film separating the two layers [10, 11] (Fig. 1). According to Nagelberg *et al.* [12], the rate of oxidation of Al–Mg–Si alloys in the growth stage is controlled by the electronic conductivity of the continuous, external, MgO layer. To investigate the role of electronic transport in the oxidation kinetics in the growth stage, DebRoy *et al.* [13] carried out directed oxidation experiments of a Al–Mg alloy (Al-5056 alloy) in which platinum wires were positioned inside the alloy so that the wires would extend through the composite matrix and the top MgO layer to facilitate electronic transport. They observed that the rate of oxidation in the growth stage was independent of the presence or absence of Pt wires indicating that the transport of electronic species does not control the oxidation kinetics of Al–Mg alloys that do not contain silicon. In view of the crucial difference in the oxidation mechanism of Al–Mg alloys with or without the presence of Si, Venugopalan *et al.* [14, 15] investigated the growth stage kinetics in the directed oxidation of Al–Mg and Al–Mg–Si alloys. They [14] concluded that, for Al–Mg alloys, oxygen transport through the thin alloy layer near the surface controlled the growth rate. Silicon additions increase the rate of oxygen transport through the alloy layer and decrease the rate of electronic transport through the MgO layer [15]. As a result, electronic transport through the outer MgO layer controls the rate of oxidation of Al–Mg–Si alloys [12, 15].

It has been recognized that the toughness of ceramic matrix composites containing ductile phases is controlled by the volume fraction and interconnection of the ductile phase [16, 17]. Aghajanian *et al.* [18] measured the mechanical properties of Al_2O_3/Al composites grown by directed melt oxidation of aluminium alloys. They observed that the flexural strength of Al_2O_3/Al composites increased with increase in the volume fraction and interconnection of Al metal channels [18]. It was also found that the critical strain energy release rate, which is a measure of the toughness, was highest for the composite which contained the largest amount of interconnected Al channels [18]. Thus, it is clearly seen that the metal distribution in Al_2O_3/Al composites needs to be tailored to ensure maximum enhancements in toughness.

Very little information is available in the literature on the procedure to tailor the metal content of Al_2O_3/Al composites prepared by directed oxidation. A notable exception is the investigation of Manor *et al.* [19] who measured the volume fraction of Al in Al_2O_3/Al composites, grown by directed oxidation of a complex Al–Zn–Mg–Si–Cu–Fe alloy at various temperatures. They observed that the volume fraction of Al in the Al_2O_3/Al composites decreased with increasing growth temperature. However, the reason for the observed dependence of the amount of metal in the composite on the growth temperature is not clearly understood. The dependence of metal interconnection in Al_2O_3/Al composites on the growth temperature has not been investigated. In addition to controlling the toughness of Al_2O_3/Al composites, the interconnection of Al metal is the basis for liquid metal transport in the growth stage by wicking to occur. The presence of narrow channels of alloy in selected microscopic sections in the oxide composite has been presented as "evidence" of the wicking process [20]. However, the observation of a few alloy channels in an arbitrarily selected microscopic section does not really constitute a rigorous proof that the narrow metal channels extend from the bulk liquid metal at the bottom all the way through the ceramic oxide matrix to the top of the oxide layer. Thus, the dependence of Al metal volume fraction and Al interconnection in Al_2O_3/Al composites on growth temperature needs to be investigated.

The electrical conductivity of an oxide matrix composite containing a random dispersion of aluminium metal would be significantly different from that of an oxide matrix containing an interconnected network of aluminium metal. A comparison of the electrical conductivities can establish the nature of the aluminium metal distribution in the composite. In this paper, the results of conductivity measurements of an Al_2O_3/Al composite over a temperature range of 450–1323 K are examined. The data are compared with the measured values of electrical conductivity of a sintered Al_2O_3–4 wt % MgO pellet to seek an improved understanding of the distribution of aluminium in the composite. In addition, Al_2O_3/Al composites are prepared at different temperatures and the metal interconnection in the composites determined by electrical conductivity measurements. Furthermore, the amount of metal in the Al_2O_3/Al composites is determined by microstructural analysis. It is shown that the metal distribution in the Al_2O_3/Al composites can be tailored by controlling the growth temperature.

2. Experimental procedure

2.1 Nature of metal distribution in Al_2O_3/Al composite

Cylindrical shaped pellets of an Al_2O_3/Al composite and sintered Al_2O_3–4 wt % MgO were prepared for electrical conductivity measurements. The Al_2O_3/Al composite was prepared by directed oxidation of a 5056 aluminium alloy for 48 h at 1273 K in air, in the thermogravimetric setup. The thermogravimetric setup consisted of a Cahn model 1000 automatic recording electric balance, a high temperature silicon carbide tube furnace, and a gas flow and pressure control system. The balance had a sensitivity of 0.5 μg and the

measurement accuracy was 0.1% of the recorder range. The quartz reaction tube was of 48 mm internal diameter and had a 25 mm equi-temperature zone at the centre of the furnace. The furnace was equipped with an electronic temperature controller which regulated the temperature to ± 5 K. The Al_2O_3–MgO pellet was prepared by sintering a mixture of fine powders, 110 μm average particle size, of 96 wt % Al_2O_3 and 4 wt % MgO at 1673 K for 48 h in an argon atmosphere.

Fig. 2 shows the experimental set-up used for measuring the electrical conductivity of the pellets using the two electrode method. The set-up consisted of an electrical conductivity cell, vertical tube furnace and an electrical conductivity measurement unit, Quad Tech RLC Digibridge Model 1689 M. The conductivity cell consisted of a gas tight alumina chamber with gas flow, thermocouple and electrical feedthroughs. The pellet was placed between the platinum foils as shown in Fig. 2. Platinum paint was applied on the flat surfaces of the sample to achieve good contact with the electrodes. Resistance measurements were made as a function of temperature by heating the samples in argon at atmospheric pressure and a gas flow rate of 500 sccm. A Pt–Pt 10% Rh thermocouple placed in close proximity to the sample was used to measure the sample temperature. The RLC Digibridge was operated at low test frequency, 12 Hz, to improve the accuracy of the readings. Furthermore, the resistance measurements were made during the time interval when no current was flowing to the furnace to minimize inductive effects on the measured impedance.

2.2 Dependence of metal distribution in Al_2O_3/Al composite on growth temperature

Al_2O_3/Al composites were grown by directed oxidation of the Al 5056 alloy in the temperature range of 1393–1612 K in the thermogravimetric set-up. SiO_2 powder was applied to the surface of the alloy to minimize the duration of incubation. In all the experiments, oxidation was carried out till the weight gain recorded was 1000 mg. Electrical conductivity measurements of the composites were conducted in the setup shown in Fig. 2 to determine the change in metal distribution as a function of the growth temperature. The temperature of conductivity measurements was kept constant at 298 K.

Microstructural characterization of the composites included optical metallography and scanning electron microscopy (SEM). Metallographic samples were sectioned with a low-speed diamond saw, ground and polished with diamond paste. SEM specimens were coated with carbon to eliminate charging under the electron beam. The amount of metal in the composites was determined from the micrographs by image analysis.

3. Results and discussion

3.1 Nature of metal distribution in Al_2O_3/Al composites

In order to understand the distribution of aluminium metal in the Al_2O_3/Al composite, electrical conductivities of Al_2O_3/Al and sintered Al_2O_3–4 wt % MgO were compared. The matrix of the Al_2O_3/Al composite typically has a few per cent of spinel [20] and some magnesium dissolved in the alumina [18]. Thus, the sintered Al_2O_3–4 wt % MgO pellet is considered to be more representative of the composite matrix than a pure alumina pellet. The measured conductivities at various temperatures are presented in Fig. 3. The results indicate that the conductivity of the Al_2O_3/Al composite is six to seven orders of magnitude higher than that of the sintered Al_2O_3–MgO pellet. The Al_2O_3/Al composite differs from the sintered Al_2O_3–MgO pellet primarily in that the composite has some aluminium metal in it. Thus, the observed higher conductivity of the Al_2O_3/Al composite can be attributed to the presence of aluminium, either as a random dispersion or in the form of interconnected channels in the alumina matrix.

The conductivity of a sintered Al_2O_3–4 wt % MgO pellet containing a random dispersion of uniform sized aluminium spheres (20 vol %), σ, can be estimated, from the conductivity of the sintered oxide

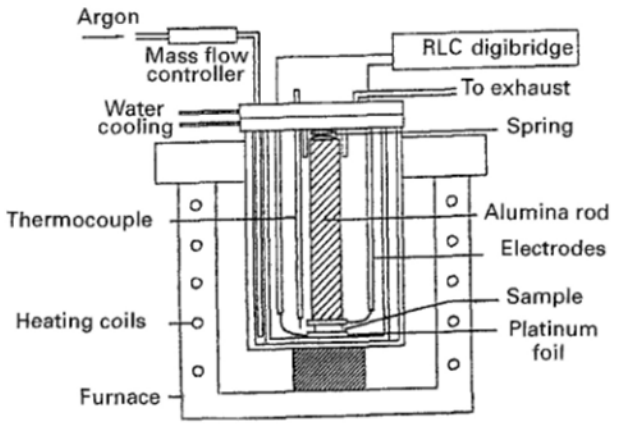

Figure 2 Schematic diagram of the experimental setup used for electrical conductivity measurements.

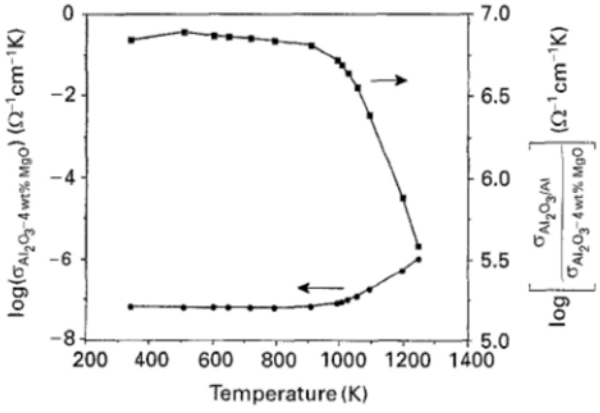

Figure 3 Electrical conductivity of Al_2O_3/Al composite and sintered Al_2O_3–4 wt % MgO at various temperatures. Measurements were made in argon at 1-atm (1.013×10^5 Pa) pressure and a gas flow rate of 500 sccm.

pellet without the metal dispersion, σ_m, using Maxwell's relation [21, 22]:

$$K_m = \frac{\sigma}{\sigma_m} = \frac{K_d + 2 - 2f(1 - K_d)}{K_d + 2 + f(1 - K_d)} \quad (1)$$

where

$$K_m = \frac{\text{conductivity of the oxide medium with dispersion}}{\text{conductivity of the oxide medium without dispersion}} \quad (2)$$

$$K_d = \frac{\text{conductivity of the dispersed phase (aluminium)}}{\text{conductivity of the oxide medium without dispersion}} \quad (3)$$

and f is the volume fraction of the dispersed phase, aluminium in this case. Since the conductivity of aluminium [23] is 12 orders of magnitude greater than the conductivity of sintered Al_2O_3–MgO, i.e. $K_d \gg 1$, Equation 1 reduces to

$$K_m = \frac{(1 + 2f)}{(1 - f)} \quad (4)$$

Breval *et al.* [20] have reported that alumina matrix composites produced by directed metal oxidation of aluminium alloys contain up to 20 vol % aluminium. Equation 4 predicts that a random dispersion of 20 vol % aluminium in sintered Al_2O_3–MgO would enhance the conductivity by a factor of 1.75. Thus, a random distribution of aluminium in the composite cannot explain the six to seven orders of magnitude higher conductivity of Al_2O_3/Al composite compared to that of sintered Al_2O_3–MgO. The result indicates the presence of aluminium as continuous channels extending through the entire thickness of the Al_2O_3/Al composite. These metal channels provide a low resistance electrical path in an otherwise high resistance oxide matrix, resulting in the observed high conductivity of the composite.

Since Al_2O_3/Al composites have continuous aluminium channels, the composites should have high electrical conductivity. It is shown in Appendix A that if the aluminium channels in the composite are assumed to be of roughly equal length and cross-sectional area, the conductivity of the composites, σ_c, is given by:

$$\sigma_c = \frac{\sigma_{Al} f_m}{\tau} \quad (5)$$

where σ_{Al} is the conductivity of aluminium. It is observed from Fig. 3 that the measured conductivity of a Al_2O_3/Al composite sample at 1000 K is 4.3×10^{-1} ohm^{-1} cm^{-1}. The conductivity of liquid aluminium at 1000 K is 4.0×10^4 ohm^{-1} cm^{-1} [23]. Thus, there is a five orders in magnitude difference in the conductivity of Al_2O_3/Al composite and aluminium. If the metal channels are assumed to be straight, i.e., $\tau = 1$, the fractional metal channel area, f_m, is found to be 1.1×10^{-5}. Since the estimated area fraction is unrealistically low, the assumptions that the channels are straight and that all channels extend over the entire thickness of the Al_2O_3/Al composite must be examined closely. In the Al_2O_3/Al composite, the metal is present as tortuous channels and not all channels extend through the entire thickness of the composite. Assuming a very high tortuosity factor of 100, a fractional channel area, f_m, of 1.1×10^{-3} is obtained. Thus, the tortuosity of the channels alone cannot explain the low area fraction. Therefore,the low conductivity of the composite in comparison with aluminium must be attributed to a composite structure where only a small fraction of the metal channels extend through the entire thickness of the composite.

A comparison of the conductivity of the composite and aluminium metal at 500 K yields a fractional channel area of 2.3×10^{-6} which is about five times lower than that calculated at 1000 K. This decrease in the fractional channel area with decrease in temperature can be explained on the basis of the large difference in the thermal expansion coefficients of aluminium and alumina. The coefficients of linear thermal expansion of solid and liquid aluminium are 30×10^{-6} K^{-1} and 41×10^{-6} K^{-1} [24] respectively, whilst that of alumina is 10×10^{-6} K^{-1} [25]. Furthermore, aluminium shrinks by 6% on solidification [24]. On cooling, this volume shrinkage and the difference in the coefficients of thermal expansion of aluminium and alumina can cause (a) reduction in the cross-sectional area of the channels and (b) discontinuities in the metal channels reducing the number of the channels that extend through the entire thickness of the composite. Although the conductivity of aluminium increases with decrease in temperature, the effect is compensated, at least in part, by the reduction in the number and cross-sectional area of the channels. The observed insensitivity of the conductivity with changes in temperature of the Al_2O_3/Al composite is consistent with these two opposing effects.

3.2. Activation energy for diffusion through Al_2O_3/Al composites

Once the bulk metal is completely exhausted, further oxidation of the metal in the channels would be expected to occur by ionic diffusion through the Al_2O_3 matrix. The determination of the activation energy of this process and the nature of the dominant charge carrier in the oxide matrix is therefore of interest. The presence of continuous aluminium channels in the Al_2O_3/Al composites precludes the determination of the dominant charge carrier in the oxide matrix from the measured electrical conductivity of the composite. Since the matrix in the Al_2O_3/Al composite is similar in chemical composition to the sintered Al_2O_3–4 wt % MgO pellet, the nature of the charge carrier in the alumina matrix can be examined using the electrical conductivity data for sintered Al_2O_3–4 wt % MgO presented in Fig. 3. Conductivity data of sintered Al_2O_3–4 wt % MgO, in the temperature range 1080–1250 K, were used to determine the activation energy for the diffusion of the dominant charge carrier. At lower temperatures, because of the very low bulk conductivity of Al_2O_3–4 wt % MgO, surface and/or gas phase conduction can result in inaccurate bulk conductivities [26]. Hence, meaningful activation energy data can not be derived from the conductivities at temperatures lower than 1000 K. The variation of $\ln \sigma T$ versus $1000/T$, commonly used to determine the activation energy for the diffusion of the dominant charge carrier [27], is presented in Table I.

TABLE I Variation of $\ln(\sigma T)$ versus $1000/T$ for sintered Al_2O_3–4 wt % MgO

$\ln(\sigma T)$, $(\Omega^{-1}\,cm^{-1}\,K)$	$1000/T$, (K^{-1})
−13.835	0.801
−14.299	0.824
−14.385	0.827
−14.500	0.835
−14.639	0.842
−14.914	0.861
−15.075	0.873
−15.205	0.884
−15.446	0.902
−15.592	0.914
−15.610	0.915
−15.732	0.925

An activation energy of 1.36 eV is obtained for the diffusion of the dominant charge carrier in Al_2O_3–4 wt % MgO. The measured activation energy of 1.36 eV is in fair agreement with a value of 1.6 eV obtained by Yee *et al.* [28] for a MgO doped polycrystalline Al_2O_3 sample and represents the activation energy for diffusion through Al_2O_3.

Yee *et al.* [28] have shown that in the temperature range of interest and for $P_{O_2} < 10^{-4}$ atm, (10.13 Pa) the transference number of ions, i.e., the ratio of the ionic conductivity and the total conductivity, is close to unity. Hence, this activation energy would correspond to the activation energy of diffusion of an ionic species. The magnesium in sintered Al_2O_3–4 wt % MgO would be in saturated solid solution in alumina and hence extrinsic ionic defects are expected to dominate. Therefore, the observed activation energy represents the migration energy of the dominant extrinsic defect in sintered Al_2O_3–4 wt % MgO. Several investigators [29–37] have attempted to identify the nature of the dominant extrinsic defect in acceptor (Mg, Fe) dominated Al_2O_3. However, there is significant controversy as to whether aluminium ion interstitials [30–33] or oxygen ion vacancies [34–37] are the dominant extrinsic defects. The activation energy, for the diffusion of the dominant charge carrier in Al_2O_3–4 wt % MgO, measured in this study could be interpreted as the migration energy of either aluminium ion interstitials or oxygen ion vacancies.

3.3. Dependence of metal distribution in Al_2O_3/Al composites on growth temperature

Electrical conductivities of Al_2O_3/Al composites, grown at different temperatures, are shown in Fig. 4. The conductivity measurements were carried out at 298 K. It can be seen that the electrical conductivity and, correspondingly, the degree of interconnection of the aluminium channels, decrease with increase in the growth temperature. SEM micrographs of the composites, grown at different temperatures, are shown in Fig. 5(a–c). EDS (Energy dispersive X-ray spectroscopy) analysis indicates that the dark grey areas are essentially Al, while the light grey areas are Al_2O_3. The black areas are pores. It is observed from

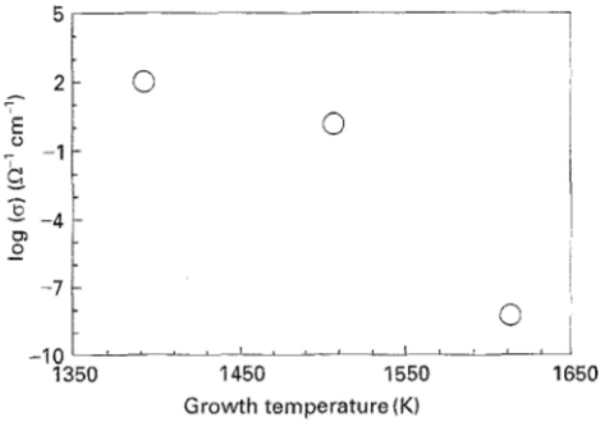

Figure 4 Electrical conductivity of Al_2O_3/Al composites, as a function of the growth temperature. Measurements were made 298 K in argon at 1-atm (1.013×10^5 Pa) pressure and a gas flow rate of 500 sccm.

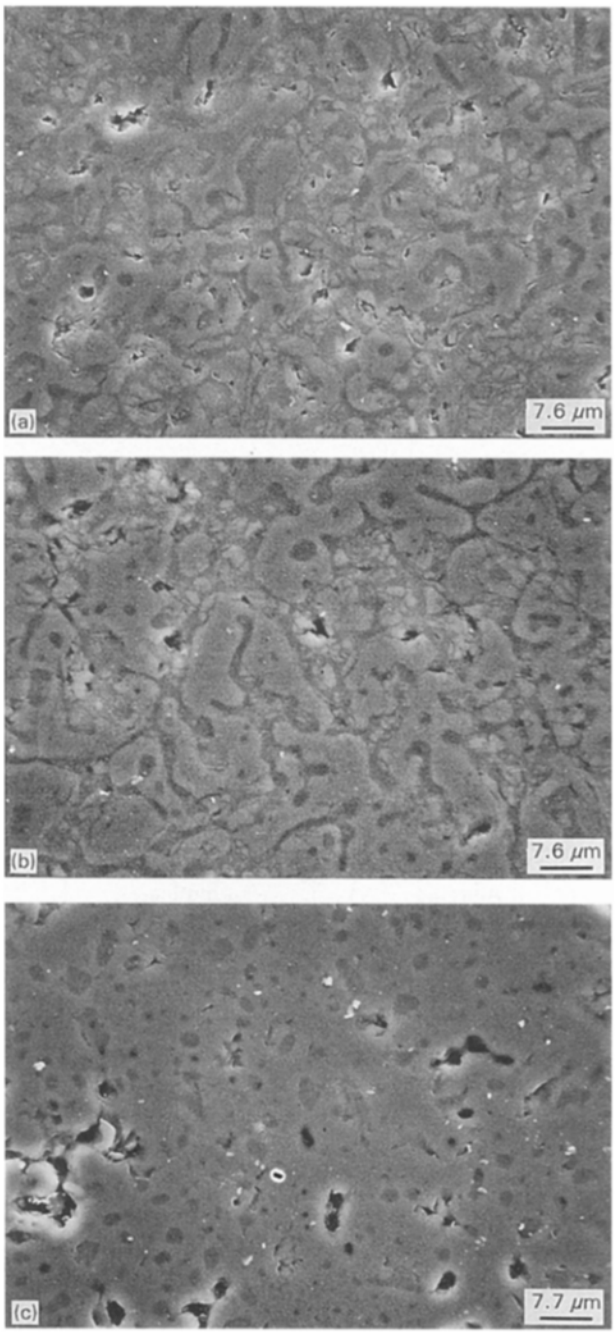

Figure 5 SEM micrographs showing the general microstructural features of composites produced by directed melt oxidation of Al-5056 alloy at different temperatures (a) 1393 K, (b) 1508 K, and (c) 1612 K.

Fig. 5(a–c) that the number of pores increases with increasing growth temperature. This is consistent with the observations of Aghajanian *et al.* [18]. The amount of metal in the composites was measured by image analysis of the micrographs. Table II shows that the volume fraction of metal in the composite decreases as a function of the growth temperature. It is noted from Table II that the proportion of metal in the Al_2O_3/Al composites could vary by as much as $\pm 6\%$. A similar scatter was observed by Manor *et al.* [19]. Thus, it is observed that both the amount of metal and the extent of metal interconnection decrease with increasing growth temperature. These experimental observations can be rationalized by arguments based on interfacial energy considerations as discussed below.

As shown in Fig 6(a and b) when Al metal penetrates through an alumina grain boundary and forms a channel, an alumina/alumina interface (grain boundary) is replaced by two liquid aluminium/alumina interfaces. For this microstructure to be stable, it is necessary that:

$$\gamma_{SS} > 2\gamma_{SL} \quad (6)$$

where γ_{SS} is the energy of a grain boundary of alumina and γ_{SL} is the interfacial energy between the molten aluminium and the solid alumina. While interfacial energies are less dependent on orientation, the energy of a grain boundary depends on the mis-orientation between the adjacent crystals [38], generally increasing asymptotically with mis-orientation [39]. Grain boundary energies range from small through intermediate values for low-angle grain boundaries to relatively high values for high angle boundaries [39]. Equation 6 indicates that the ceramic component of Al_2O_3/Al composites may interconnect along low angle grain boundaries but be separated by metal channels along high angle grain boundaries. Indeed, transmission electron microscopy studies [1, 20] reveal that low angle Al_2O_3–Al_2O_3 grain boundaries are free of second phases. It was also observed by Newkirk *et al.* [1] that high-angle grain intersections contained thin channels of Al metal separating neighbouring Al_2O_3 crystals rather than a high angle Al_2O_3–Al_2O_3 grain boundary. Since Al_2O_3 crystals produced by directed oxidation grow with their *c*-axis nearly parallel to the growth direction [20], grain boundaries nearly parallel to the *c*-axis must be considered. As the number of such boundaries for which Equation 6 is satisfied increase, the number of metal channels and correspondingly, the electrical conductivity of the Al_2O_3/Al composite would increase. Values for γ_{SL} can be obtained from experimental data [40, 41]. Several grain boundary orientations are possible for which the grain boundary is nearly parallel to the *c*-axis [42]. However, experimental values for all these orientations are not available. For a $\Sigma 11$ grain boundary in alumina ([21, 10] 35.2° tilt boundary mis-orientation), experimental values of γ_{SS} are available. High resolution transmission electron microscopy studies of Hoche *et al.* [43] reveal that γ_{SS} is $1.7\,J\,m^{-2}$ at 1893 K. By extrapolation, γ_{SL} is $0.549\,J\,m^{-2}$ at a temperature of 1893 K [40, 41]. Thus, at 1893 K, it can be seen that $\gamma_{SS} > 2\gamma_{SL}$ for the $\Sigma 11$ boundary, and hence, metal would be expected to penetrate along the $\Sigma 11$ boundary.

The observed changes in the electrical conductivity with growth temperature can be explained if metal interconnection decreases with temperature i.e., γ_{SS} decreases faster relative to $2\gamma_{SL}$, for a number of grain boundaries with increase in growth temperature. Thus, more ceramic–ceramic grain boundaries would become stable as the growth temperature increases. The decrease in the number of alumina grain boundaries through which aluminium can penetrate would explain the decrease in the amount and interconnection of metal in the composite with increasing processing temperature. However, energy data for various grain boundaries in alumina (parallel to the *c*-axis) and their dependence on temperature are not available. It is proposed that γ_{SS} decreases faster than $2\gamma_{SL}$ with increase in temperature though experimental data on grain boundary energies in alumina are yet to be obtained. The present argument draws on interfacial energy relationships similar to those worked out to explain grain boundary microstructures in other ceramic–metal systems such as WC–Co, WC–Cu, Si_3N_4-glass and SiC–Si [44–46].

TABLE II Volume fraction of Al metal in Al_2O_3/Al composites as a function of the growth temperature

Growth temperature (K)	Volume fraction of metal (%)
1393	19.5 ± 6
1508	14.0 ± 4.5
1612	7.7 ± 3

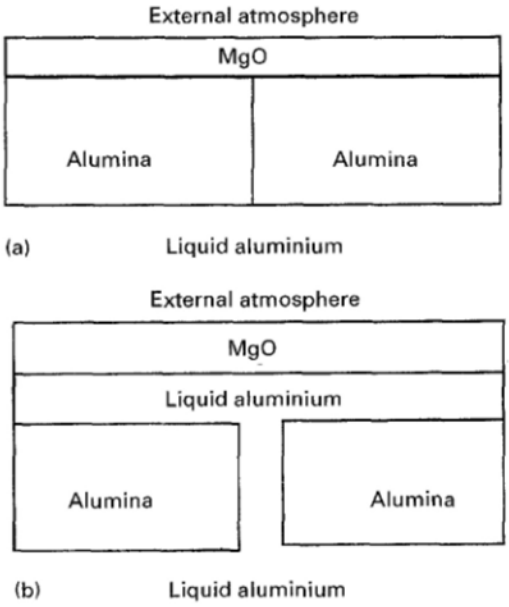

Figure 6 Schematic description of condition for formation of metal channels. (a) Metal channels cannot form ($\gamma_{SS} < 2\gamma_{SL}$). (b) Metal channels can form in the grain boundary ($\gamma_{SS} > 2\gamma_{SL}$).

4. Conclusions

Electrical conductivities of Al_2O_3/Al composite and Al_2O_3–MgO pellets were used to understand the

distribution of aluminium metal in the Al_2O_3/Al composite and the activation energy for the migration of the dominant charge carrier in the alumina matrix. The conductivity of the Al_2O_3/Al composite was found to be six to seven orders of magnitude higher than that of sintered Al_2O_3–4 wt % MgO. A small fraction of the aluminium channels extend over the entire thickness of the composite. The activation energy of migration of the dominant charge carrier in the sintered Al_2O_3–4 wt % MgO was found to be 1.36 eV.

The electrical conductivity of the Al_2O_3/Al composite and the amount of metal in the composite were studied as a function of the growth temperature to understand the temperature dependence of metal distribution in the composite. The results indicate that both the quantity and interconnection of the Al phase in the Al_2O_3/Al composite decrease with increasing growth temperature. The observed changes in microstructure with temperature can be explained if γ_{SS} decreases faster relative to $2\gamma_{SL}$, for a number of grain boundaries in Al_2O_3, as the growth temperature increases.

Appendix A
Determination of electrical conductivity of an Al_2O_3/Al composite containing tortuous Al channels

Consider an Al_2O_3/Al composite containing Al metal in the form of channels of varying tortuosities as shown in Fig. 7. The resistances of the various Al metal channels, R_1, are given by the following expressions:

$$R_1 = \frac{\rho_{Al} L_1}{A_1}, \qquad R_2 = \frac{\rho_{Al} L_2}{A_2}, \qquad R_n = \frac{\rho_{Al} L_n}{A_n} \tag{A1}$$

where L_i denotes the length of channel i, A_i the area of channel i, and ρ_{Al} denotes the resistivity of Al. The total resistance of the composite, R_c, is given by the expression:

$$\frac{1}{R_c} = \frac{A_c}{\rho_c L_c} = \frac{A_1}{L_1 \rho_{Al}} + \frac{A_2}{L_2 \rho_{Al}} + - + - + - + \frac{A_n}{L_n \rho_{Al}} \tag{A2}$$

where A_c denotes the total cross-sectional area of the composite, L_c the thickness of the composite, and ρ_c denotes the resistivity of the composite. If the metal channels are assumed to be of equal length and cross-sectional area, i.e., $A_1 = A_2 = \cdots = A_n = A_i$, and $L_1 = L_2 = \cdots = L_n = L_i$, Equation A2 can be simplified as:

$$\rho_c = \frac{\rho_{Al} L_i A_c}{n A_i L_c} = \frac{\rho_{Al} \tau}{f_m} \tag{A3}$$

where $\tau = L_1/L_c$ = tortuosity factor and f_m is the fractional metal channel area given by:

$$f_m = \frac{n A_i}{A_c} \tag{A4}$$

It follows from Equation A3 that the conductivity of the composite, σ_c, is given by:

$$\sigma_c = \frac{\sigma_{Al} f_m}{\tau} \tag{A5}$$

where σ_{Al} denotes the conductivity of aluminium.

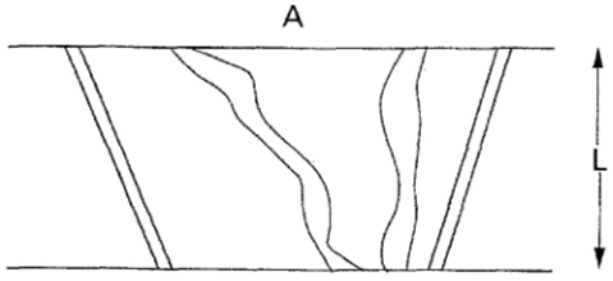

Figure 7 Schematic representation of metal channels in an Al_2O_3/Al composite.

Acknowledgements

This work was supported by the National Science Foundation under Grant no. DMR-9118075. The authors wish to thank Prof. R. Roy for his interest in the work. We would like to thank Dr. K. Tankala for useful discussions and Mr. T. Rusnak for help with the SEM.

References

1. M. S. NEWKIRK, A. W. URQUHART, H. R. ZWICKER and E. BREVAL, *J. Mater. Res.* **1** (1986) 81.
2. M. S. NEWKIRK, H. D. LESHER, D. R. WHITE, C. R. KENNEDY, A. W. URQUHART, and T. D. CLAAR, *Ceram. Eng. Sci. Proc.* **8** (1987) 879.
3. C. A. ANDERSSON, P. BARRON-ANTOLIN, G. H. SCHIROKY and A. S. FAREED, In "*Whisker and Fibre Toughened Ceramics*", edited by R. A. Bradley (ASM International, Materials Park, OH, Warresodale, 1988) pp 209–215.
4. A. S. NAGELBERG, A. S. FAREED and D. J. LANDINI, in "Processing and Fabrication of Advanced Materials", V. A. Ravi and T. S. Srivatsan (eds.) (The Minerals, Metals and Materials Society, 1992) pp 127–142.
5. A. W. URQUHART, *Mater. Sci. Engng* **A144** (1991) 75.
6. A. S. NAGELBERG, *Solid State Ionics* **32/33** (1989) 783.
7. K. C. VLACH, O. SALAS, H. NI, V. JAYARAM, C. G. LEVI and R. MEHRABIAN, *J. Mater. Res.* **6** (1991) 1982.
8. H. VENUGOPALAN, K. TANKALA and T. DEBROY, *Metall. Mater. Trans.* **27B** (1996) 43.
9. O. SALAS, V. JAYARAM, K. C. VLACH, C. G. LEVI and R. MEHRABIAN, *J. Amer. Ceram. Soc.* **78** (1995) 609.
10. O. SALAS, H. NI, V. JAYARAM, K. C. VLACH, C. G. LEVI and R. MEHRABIAN, *J. Mater. Res.* **6** (1991) 1964.
11. S. ANTOLIN, A. S. NAGELBERG and D. K. CREBER, *J. Amer. Ceram. Soc.* **75** (1992) 447.
12. A. S. NAGELBERG, S. ANTOLIN and A. W. URQUHART, *ibid*, **75** (1992) 455.
13. T. DEBROY, A. BANDHOPADHYAY and R. ROY, *ibid*, **77** (1994) 1296.
14. H. VENUGOPALAN, K. TANKALA and T. DEBROY, *Mater. Sci. Engng. A.* **21011-2** (1996) 64.
15. H. VENUGOPALAN and T. DEBROY, *J. Eur. Ceram. Soc.* (in press).
16. L. SIGL, P. MATAGO, B. J. DALGLEISH, R. M. MCMEEKING and A. G. EVANS, *Acta Metall.* **36** (1988) 945.
17. C. A. ANDERSSON and M. K. AGHAJANIAN, *Ceram. Eng. Sci. Proc.* **9** (1988) 621.
18. M. K. AGHAJANIAN, N. H. MACMILLAN, C. R. KENNEDY, S. J. LUSZCZ and R. ROY, *J. Mater. Sci.* **24** (1989) 658.

19. E. MANOR, H. NI, C. G. LEVI and R. MEHRABIAN, *J. Amer. Ceram. Soc.* **76** (1993) 1777.
20. E. BREVAL, M. K. AGHAJANIAN and S. J. LUSZCZ, *Ibid*, **73** (1990) 2610.
21. R. E. MEREDITH and C. W. TOBIAS, in "*Adv. Electrochem. Electrochemical Engng.*, **2**," edited by F. W. Tobias (Interscience, New York, 1962) p 15.
22. L. K. H. VON BEEK, in "Progress in Dielectrics," **7**, F. B. Birks and F. H. Schulman (eds.) (Heywood, London, 1965) p 69.
23. E. A. BRANDES and G. B. BROOK (Eds.), "*General Physical Properties: Smithells Metals Reference Handbook*," 7th Edn (Butterworth Heinemann, London, UK, 1992) p 14.
24. A. R. UBBELOHDE, "*The Molten State of Matter*" (Wiley, New York, 1978) p 239.
25. W. D. KINGERY, H. K. BOWEN and D. R. UHLMANN, "*Introduction to Ceramics*," 2nd Edn. (Wiley, New York, 1976) p 593.
26. A. J. MOULSON and P. POPPER, *Proc. Brit. Ceram. Soc.* **10** (1968) 41.
27. P. KOFSTAD, *in* "*Nonstoichiometry. Diffusion and Electrical Conductivity in Binary Metal Oxides*," (Wiley-Interscience, New York, 1972) p 87.
28. J. YEE and F. A. KROGER, *J. Amer. Ceram. Soc.* **56** (1973) 189.
29. F. A. KROGER, in "*Structure and Properties of MgO and Al_2O_3 Ceramics*" edited by W. D. Kingery (American Ceramic Society, Columbus, OH, 1984) pp 100–118.
30. B. V. DUTT and F. A. KROGER, *J. Amer. Ceram. Soc.* **58** (1975) 474.
31. M. M. EL-AIAT, L. D. HOU, S. K. TIKU, H. A. WANG and F. A. KROGER, *ibid*, **64** (1981) 174.
32. G. W. HOLLENBERG and R. S. GORDON, *ibid*, **56** (1973) 140.
33. R. T. COX, *J. Phys.* (*Paris*). *Colloq.* **34** (1973) 333.
34. B. J. PLETKA, T. E. MITCHELL and A. H. HEUER, *Acta Metall* **30** (1982) 147.
35. W. RAJA RAO and I. B. CUTLER, *J. Amer. Ceram. Soc.* **56** (1973) 588.
36. S. K. MOHAPATRA, S. K. TIKU and F. A. KROGER, *ibid* **62** (1979) 50.
37. K. KITZAWA and R. L. COBLE, *ibid*, **57** (1974) 245.
38. G. A. CHADWICK and D. A. SMITH, "*Grain Boundary Structure and Properties*," (Academic Press, London, 1976).
39. W. BOLLMANN, "*Crystal Defects and Crystalline Interfaces*" (Springer, Berlin, 1970).
40. V. LAURENT, D. CHATAIN, C. CHATILLON and N. EUSTATHOPOULOS, *Acta Metall.* **36** (1988) 1797.
41. L. D. LUCAS, "*Techniques de l'Ingenieur*" (M67 Paris, 1984).
42. H. GRIMMER, R. BONNET, S. LARTIGUE and L. PRIESTER, *Philos. Mag.* **A61** (1990) 493.
43. T. HOCHE, P. R. KENWAY, H. J. KLEEBE, M. RUHLE and P. A. MORRIS, *J. Amer. Ceram. Soc.* **77** (1994) 339.
44. D. R. CLARKE and G. THOMAS, *Ibid*, **60** (1977) 491.
45. W. P. MINNEAR, *Ibid*, **65** (1982) C-10.
46. N. M. PARIKH and M. HUMENIK, *ibid*, **40** (1957) 315.

Received 20 September 1995
and accepted 15 January 1996